Solar Phys (2008) 248: 51–65
DOI 10.1007/s11207-008-9127-6

Where Do Solar Filaments Form?: Consequences for Theoretical Models

Duncan H. Mackay · Victor Gaizauskas · Anthony R. Yeates

Received: 10 August 2007 / Accepted: 11 January 2008 / Published online: 3 February 2008

Abstract This paper examines the locations where large, stable solar filaments form relative to magnetic bipoles lying underneath them. The study extends the earlier work of F. Tang to include two additional classification categories for stable filaments and to consider their population during four distinct phases of the solar cycle. With this new classification scheme, results show that over 92% of filaments form in flux distributions that are nonbipolar in nature where the filament lies either fully (79%) or partially (13%) above a polarity inversion line (PIL) external to any single bipole. Filaments that form within a single bipole (traditionally called Type A) are not as common as previously thought. These results are a significant departure from those of F. Tang. Consistency with the earlier work is shown when our data are regrouped to conform to the two-category classification scheme for filaments adopted by F. Tang. We also demonstrate that only filaments that form along the external PIL lying between two bipoles (62% of the full sample, traditionally called Type B) show any form of solar cycle dependence, where their number significantly increases with magnetic activity over the solar cycle. Finally, current observations and theoretical models for the formation of filaments are discussed in the context of the present results. We conclude that key elements in the formation of the majority of filaments considered within this study must be the convergence of magnetic flux resulting in either flux cancellation or coronal reconnection.

Keywords Prominences: Formation and evolution · Prominences: Models

D.H. Mackay (✉) · A.R. Yeates
School of Mathematics and Statistics, University of St. Andrews, North Haugh, St. Andrews KY16 8HB, UK
e-mail: duncan@mcs.st-and.ac.uk

A.R. Yeates
e-mail: anthony@mcs.st-and.ac.uk

V. Gaizauskas
Herzberg Institute of Astrophysics, National Research Council of Canada, Ottawa, Ontario K1A OR6, Canada
e-mail: vicgz@rogers.com

1. Introduction

Solar filaments (also known as prominences) form over a wide range of latitudes on the Sun. Their locations spread everywhere, from the active belts to the polar crown (McIntosh, 2002; Minarovjech, Rybansky, and Rusin, 1998; Ambrož and Schroll, 2002; Mouradian and Soru-Escaut, 1994). Although solar filaments may form at many locations on the Sun, they always form above polarity inversion lines (PILs), which divide regions of positive and negative flux. Observations show that magnetic fields are key to the existence of solar filaments (Mackay, 2005) and that the dominant direction of the magnetic field within a filament is mainly along its long axis (Leroy, 1989).

To understand the role that magnetic fields play in filament formation it is important to understand the type of magnetic configurations wherein filaments form. One early classification scheme splits them into two categories (Tang, 1987). These are based on the nature of the PIL above which the filament lies. The first category, in which the filament forms above a PIL lying within a single bipolar unit of flux, is classified as a *bipolar region filament*. In the second, the filament forms above a PIL that lies in between two separate magnetic bipoles and is called a *between bipolar region filament*. Tandberg-Hanssen (1995) describes these two categories as Type A and Type B, respectively. Observations by Tang (1987) have shown that over 60% of filaments form between bipolar regions (Type B; see also Gaizauskas and Zwaan, 1997).

The aim of the present paper is to reconsider where large, stable solar filaments form with respect to PILs inside and outside individual magnetic bipoles. As this study is directed towards large, stable filaments, we disregard small, unstable filaments such as those forming in the centres of activity complexes. In contrast to Tang (1987) who studied two years (cycle minimum and maximum) the present study will be carried out over four distinct phases of the solar cycle. In addition, two new categories for filaments are introduced. These new classifications are required to distinguish the different bipole interactions and physical processes that may lead to the formation of filaments. In addition the results will be compared with currently published theoretical models to determine which are most applicable to describe filament formation. Understanding where filaments form throughout the solar cycle is not only important for the study of solar filaments but is a critical aspect for other phenomena such as coronal mass ejections (Li and Luhmann, 2006).

As filaments form over a wide variety of locations on the Sun it is expected that no one model will be able to explain all classifications. By comparing the locations of filament formation with theoretical models, we aim to determine which models apply to different classifications and subsequently which are best suited to explain the majority of filaments on the Sun. In addition we will search for a cycle variation in the formation mechanism of filaments. The structure of the paper is as follows. In Section 2 the data sets and classification scheme are described. The results are presented in Section 3. In Section 4, present observations and theoretical models of filament formation are discussed and the results of this paper are interpreted in terms of these models and observations. Finally in Section 5 the conclusions and future observing programs to understand the formation of filaments are outlined.

2. Data Sets and Classification Schemes

2.1. Data Sets and Method of Analysis

To categorise the locations where solar filaments form, data sets are chosen to represent four distinct phases of the solar cycle. These four phases cover the following six-month peri-

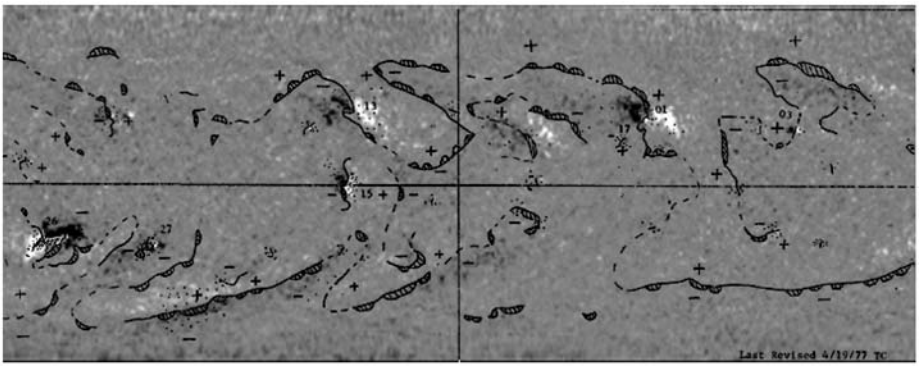

Figure 1 Example of a Kitt Peak synoptic magnetogram for CR 1653 where white represents positive flux and black negative flux. The saturation level is set at ± 50 G. Superimposed on this image are the locations of Hα filaments (hatched areas) and polarity inversion lines digitised from Solar Geophysical Data.

ods of cycle 21: March – August 1977 (CR 1653 – 1658, Set 1); March – September 1979 (CR 1680 – 1685, Set 2); March – September 1982 (CR 1720 – 1725, Set 3); and April – September 1984 (CR 1747 – 1752, Set 4). They represent the early rise phase, the rise phase near maximum, the declining phase after maximum, and the declining phase towards minimum. Cycle 21 is used rather than any later cycle because the Hα synoptic maps in Solar Geophysical Data, used to identify the positions of filaments, are extremely accurate during this cycle. Furthermore, the positions of filaments may be compared, where necessary, to those found in Hα data archives of the Ottawa River Solar Observatory. As Solar Geophysical Data are used to identify the positions of the filaments this study is preferentially directed towards large, stable filaments. Therefore, many short-lived, unstable filaments forming in the centres of active regions are ignored. For these four phases the following data are considered:

1. Hα *synoptic maps* from Solar Geophysical Data: These are used to determine the location of Hα filaments and the PILs they overlie. The total number of filaments identified in each set are 101, 234, 149, and 119, where approximately equally numbers are found in each hemisphere.
2. *He 10830 synoptic images from NSO/Kitt Peak*: These images are used to confirm the location of filament outlines in the Hα synoptic maps.
3. *Synoptic magnetograms from NSO/Kitt Peak*: The magnetograms give the large-scale radial field distribution at the photosphere. To determine the spatial relationship between the filaments and the large-scale radial field, the Hα maps are digitised and superimposed onto the synoptic magnetograms (Figure 1). An excellent agreement is found among the filaments, the paths of the PILs, and the underlying magnetic polarities.
4. *High-resolution full-disk magnetograms from Kitt Peak*: Once the filament locations have been identified from the composite Hα and Kitt Peak synoptic maps (Figure 1) an analysis of the polarities underlying each filament is carried out using the high-resolution full-disk magnetograms.
5. *Simulations of the radial field*: As an additional data set, simulations of the radial magnetic field at the photosphere under the combined effects of flux transport and flux emergence are carried out. The simulations, utilizing the technique developed by Yeates, Mackay, and van Ballegooijen (2007), consider the evolution of the radial field component between synoptic magnetograms that are approximately 27 days apart. By storing

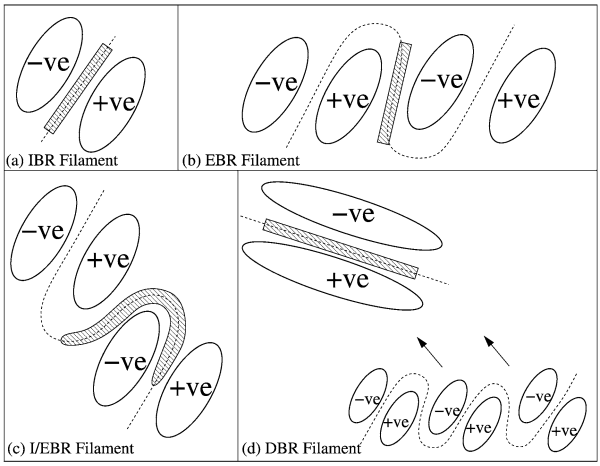

Figure 2 Classification scheme for solar filaments based on those of Tang (1987) and Tandberg-Hanssen (1995) where two new categories (c and d) are introduced. (a) Filaments that form above the internal PIL of a single bipole are classified as IBR. (b) Those forming on the external PIL between bipoles or between bipoles and unipolar regions of flux are classified as EBR. (c) Filaments that lie both above the internal PIL within a bipole and the external PIL outside the bipoles are classified as I/EBR. (d) Finally, those filaments that form in diffuse bipolar distributions where these distributions are formed through multiple flux emergence and the diffuse region can no longer be associated with any single bipole emergence are classified as DBR. This category is expected to lie only at high latitudes.

the data once every day this allows the source regions at low latitude for flux at higher latitudes to be determined.

6. *Large-scale* Hα *images from the archive of the Ottawa River Solar Observatory.*

2.2. Classification Scheme

To determine the locations where solar filaments form, a classification scheme based around that formulated by Tang (1987) and Tandberg-Hanssen (1995) is used. During the preliminary study of Gaizauskas and Zwaan (1997), it was determined that the two categories previously used could not categorise all filaments. We have accordingly introduced two new categories. The four categories defined in this paper are illustrated through a schematic diagram in Figure 2 along with Hα and magnetogram images in Figure 3. In Figure 3, the bottom image in each of the four panels shows Hα observations from the Ottawa River Solar Observatory (ORSO); the top image shows portions of either (a) – (c) the full-disk normal component or (d) the synoptic magnetograms from Kitt Peak. Outlines of the Hα filaments are superimposed onto the magnetograms to show the relative positions of each of the filaments with respect to the underlying magnetic polarities. The four classifications are as follows:

1. Filaments that form within a single magnetic bipole above the internal PIL (Figures 2(a) and 3(a)). These are the same as the bipolar region or Type A filaments of Tang (1987) and Tandberg-Hanssen (1995). In this paper they are referred to as *internal bipolar region (IBR) filaments*.
2. Filaments that form above a PIL that lies either in between two bipolar regions (Figures 2(b) and 3(b)) or between a bipolar region and a unipolar region of flux. These are

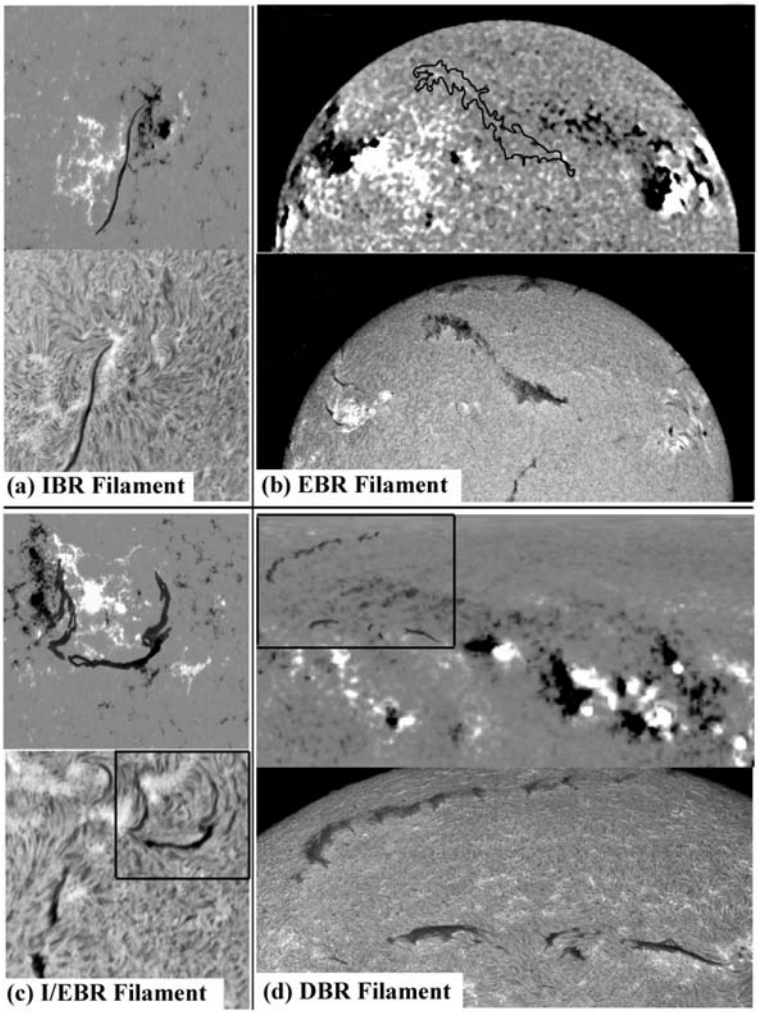

Figure 3 Examples of the four separate classifications of filaments. In each of the panels, (a)–(d), the bottom plot is an Hα image from the Ottawa River Solar Observatory and the top image shows a portion of either (a)–(c) the full-disk normal component or (d) the synoptic magnetograms from Kitt Peak. Outlines of the Hα filaments are superimposed on each of the magnetograms. The dates of the observations are (a) 26 June 1979, (b) 6 May 1979, (c) 27 September 1979, and (d) 14 July 1979. For panels (c) and (d) the areas enclosed by the boxes denote the corresponding area of (c) the magnetogram and (d) the Hα image. In panel (d) (top image) one can clearly see the low-latitude activity complexes, which will extend poleward over time and interact to produce diffuse regions of flux at high latitudes.

referred to as *external bipolar region (EBR) filaments* (previously classified as between bipolar region filaments or Type B).

3. Those filaments that are found to lie above both the internal PIL of a bipole and the external PIL surrounding the bipole (Figures 2(c) and 3(c)). As they are a mixture of the first two classes they are referred to as *internal/external bipolar regions (I/EBR) filaments*.
4. Those filaments that overlie a PIL located in essentially a bipolar distribution of flux, but where the polarities defining the bipole did not emerge together. The formation of

the bipolar distribution is the result of many flux emergences, coalescences, and cancellations such that the polarities on either side of the filament cannot be attributed to a single bipole emergence (Figures 2(d) and 3(d)). Such filaments and underlying flux distributions are only expected to occur at high latitudes above the sunspot belts. This class is distinguished from internal bipolar region filaments because the process through which the filament forms may be fundamentally different. These are referred to as *diffuse bipolar region (DBR) filaments*.

In defining any filament as belonging to one of these four categories, the history of the PIL above which the filament forms is tracked backwards to determine the origin of the source flux regions lying on either side. Therefore a filament will always be classified as IBR if it forms on the internal PIL of a bipole even if it lies at high latitudes, as long as the flux on either side can be tracked back to a single bipole emergence at low latitudes. This tracking procedure, which is distinct from previous studies, is possible because of flux transport simulations. An example of the use of this tracking procedure can be seen in Figure 4. In Figure 4(a) a portion of the Kitt Peak synoptic magnetogram for April 1979 can be seen situated in the southern hemisphere (with white/black representing positive/negative flux and north/south lying at the top/bottom of the image). On top of this image, contours of two filaments taken from Solar Geophysical Data are superimposed. The filaments lie above a switchback of the PIL where the southmost filament lies at constant latitude on the switchback lead arm (LA) and the other filament lies on the return arm (RA), which cuts through a number of latitude bands. The switchback is enclosed by positive flux and the day of year (DOY) corresponding to its central meridional passage is day 113. From the magnetogram it is not clear which polarities constitute which bipoles and which polarities are internal to any one bipole and which are external. In Figures 4(b)–(e) the results of the flux transport simulations can be seen; these simulations fill in the 27-day gap between the previous synoptic magnetogram and the one shown in Figure 4(a). In each of the plots the TV image shows the distribution of the radial field (with white/black representing positive/negative flux). On top of this image are contours of the radial field where the black solid lines represent positive flux, white dotted lines negative flux, and the white dashed line the PIL. Note that the white/black colour scale has been reversed between the TV image and the contours. The simulation results are shown in terms of a transformed coordinate system used within the simulations, which accounts for their slightly different shape and appearance. The simulations start on DOY 79 but the first image shown is on DOY 83 (Figure 4(b)), over one full rotation before the filaments were observed. It is clear from the simulation on DOY 83 that the filaments will form in a region of strong magnetic activity where there are a number of activity complexes. From this day a number of individual bipoles may be identified. In particular, two bipoles are labelled and their evolution is followed. These are labelled P1/N1 and P2/N2 for the positive and negative polarities of the two bipoles. By using the flux transport simulations the evolution of the radial field may be followed as differential rotation shears it in an east–west sense, meridional flow pushes it poleward, and diffusion leads to the cancellation of flux. Over the period of DOY 83 to DOY 113 no significant new emergences occur in the region of interest. From studying the simulations on DOY 91 and 103 (Figure 4(c) and (d)) it can be seen that a significant amount of P2 cancels with N1 and N2. In addition, as N2 lies at a slightly higher latitude, the effect of differential rotation is greater and it is sheared a larger amount in the east–west direction. With this it extends further to the left than polarity P2. By DOY 113 the spatial separation of P2 and N2 is clear with P2 containing much less flux than N2 because it has been cancelling with N1. On DOY 113 the contours of the filaments are superimposed on the image, where the cusp of the switchback is placed at its observed longitude and latitude as seen on Solar Geophysical

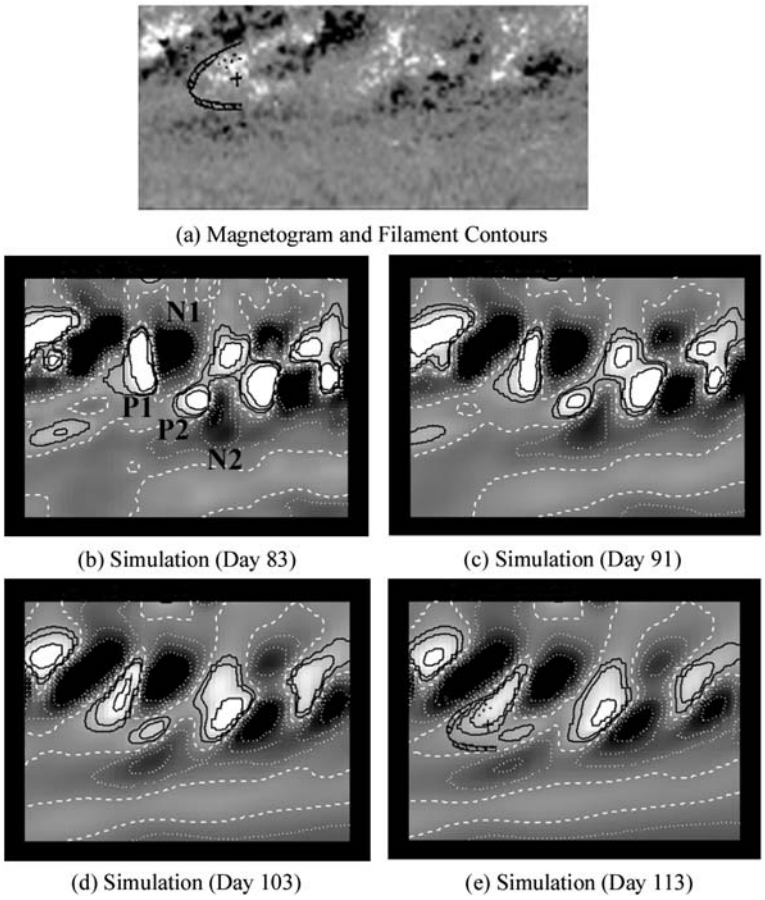

Figure 4 (a) Kitt Peak synoptic magnetogram for April 1979 showing a portion of the flux distribution in the southern hemisphere along with the contours of filaments taken from Solar Geophysical Data. The location of the filament corresponds to central meridional passage on DOY 113. (b) – (e) Simulations of the same area for DOY 83, 91, 103, and 113. In each plot the TV images show the distribution of radial magnetic field where white/black represents positive/negative flux. Superposed on the TV image are contours of the radial magnetic, where black solid contours represent positive flux, white dotted contours negative flux, and white dashed contours the PIL. On the final image, which corresponds to DOY 113, the contours of the filaments are also shown.

Data. From this image it can be seen that the filament on the lower latitude return arm lies between polarity P1 and a negative region to its left and therefore is an EBR filament. Correspondingly, the filament on the lead arm lies between polarity P1 and N2 and is therefore another EBR filament.

3. Classification of Filaments Relative to Underlying Magnetic Polarities

In Figure 5 the graph shows the number of filaments as a function of (data) set number. For each set, the plus signs denote the number in each category and the varying line styles joining these points illustrates the general outline of the curves. Cycle maximum lies midway

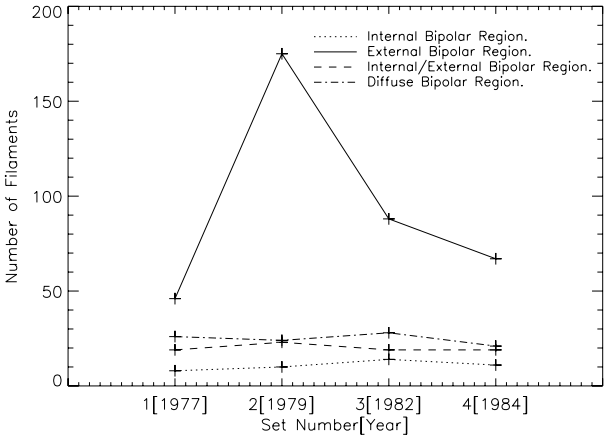

Figure 5 Graph of number of filaments in each category defined relative to the underlying photospheric flux distributions as a function of the phase of the solar cycle. The pluses denote the numbers in each category; the lines show the overall shape of the curves. Each of the different categories are shown with a different line style.

Table 1 Percentage of filaments lying within each category calculated over all four data sets along with their latitude ranges.

Filament type	Percentage of filaments	Mean latitude	Latitude range
IBR	7.13	19°	±40°
EBR	62.35	25°	±50°
IEBR	13.27	25°	±50°
DBR	16.42	55°	±40° – 70°
U	0.829		

between Sets 2 and 3. For each of the four data sets a similar behaviour is found. EBR filaments (solid line) dominate by far. They are followed in decreasing order by DBR filaments (dash-doted line), I/EBR filaments (dashed line), and finally IBR filaments (dotted line). This graph clearly shows that filaments prefer to form in flux systems involving multiple bipole interactions rather than just a single flux system.

A surprising feature of this graph is that throughout the cycle only EBR filaments show a strong variation, with all other classifications remaining approximately constant. This indicates that the formation mechanism for these must be closely related to the number of bipoles on the Sun throughout the solar cycle.

Table 1 shows the exact percentage in each category calculated over the combined data sets. According to Table 1 over 92% of all filaments occur in flux distributions that are nonbipolar in nature and require the interaction of two or more bipoles. Filaments that form in single bipolar regions along the internal PIL are not as common as previously supposed. Expanding the classification scheme for filaments beyond just two categories sheds new light on the kinds of bipole interactions most commonly associated with filaments. The final row in Table 1 shows the percentage of filaments ($\sim 1\%$) that could not be classified into any of the categories shown in Figure 2. It is clear that this number is too low to significantly alter the other percentages shown in Table 1 or the conclusions drawn from it.

The final two columns of Table 1 show the range of latitudes where filaments belonging to each of the separate classifications are found. IBR filaments all lie exclusively within the active region belt with a mean latitude calculated in each hemisphere of $\pm 19°$. In contrast EBR filaments are found to have a much wider range of latitudes ($\pm 50°$) with a higher

Table 2 Ratios used in the comparison of the results with those of Tang (1987).

Set	[IBR + I/EBR + DBR]/[EBR]
1	1.163
2	0.34
3	0.694
4	0.763

average latitude of $\pm 25°$. The I/EBR filaments follow a very similar behaviour to the EBR filaments, whereas the DBR filaments all lie at high latitudes, as expected.

Table 2 compares our results with those of Tang (1987). As two new categories have been introduced here a direct comparison is not possible. To do so, the four categories used in the present paper are reduced by calculating the ratio

$$\frac{[\text{IBR} + \text{I/EBR} + \text{DBR}]}{[\text{EBR}]}.$$

This assumes that the two new classification types introduced here are included in the "bipolar region filament" classification of Tang (1987).

The two years considered in Tang (1987) are 1973 (late declining phase of cycle 20) and 1979 (cycle maximum of cycle 21). The ratios of filaments in bipolar regions versus those in between bipolar regions as defined in Tang (1987) were 0.83 and 0.51, respectively. Although none of our present data sets represent cycle 20, Set 4 lies close enough to cycle minimum of cycle 21 that its ratio can be compared to that found by Tang (1987). The ratio of the reduced data sets found in Table 2 is 0.763, which is very similar to that found by Tang (1987) for the previous cycle. The slightly lower ratio obtained here may result from the fact that it is calculated somewhat earlier on in the cycle. This is consistent with the ratio for Set 1 being higher than that in Tang (1987), thereby showing the correct trend. For the year 1979, Tang (1987) obtained a ratio of 0.51, whereas our corresponding result is 0.34. The reason for this difference is unclear. It may arise while classifying filaments. Simulations of the surface field are used to backtrack the flux regions to determine their origin and history. In some cases this resulted in filaments that at a single instance appeared to be IBR filaments being correctly classified as EBR filaments as the polarities on either side originated from two different bipoles. When considered in the context of two classifications the results of the present study are in broad agreement with those of Tang (1987).

4. Discussion

We begin by considering observational (Section 4.1) and theoretical (Section 4.2) aspects of filament formation separately. We then proceed to make the best fit between the present results and theoretical models (Section 4.3).

4.1. Observations of Filament Formation

One of the reasons why so many filament formation models exist is that very few examples of filament formation have ever been observed. Therefore the exact formation mechanism remains debatable. Two recent publications have presented detailed case studies of filament channel and filament formation: Gaizauskas *et al.* (1997) and Gaizauskas, Mackay, and

Harvey (2001). Both cases show the formation of long, stable filaments such as the type considered in Section 3 from Solar Geophysical Data. In the first case, an intermediate filament (IF) forms over a short period of a few days; in the second a quiescent filament (QF) forms over a period of months. In both cases these filaments form on PILs external to any single bipole and would be classified here as EBR filaments.

Although the two cases occur over very different time and length scales there are a number of important similarities (as discussed in Mackay, 2005). Both cases begin with the emergence of a significant amount of magnetic flux in the form of an activity complex. Within the activity complex a significant amount of magnetic helicity is seen to emerge. This helicity produces a preferred direction of the axial field above the PIL and leads to the formation of a filament channel. Importantly, however, no filaments form during the process of flux emergence. In fact, for the large-scale QF, the filament forms 27 days after the major flux emergence subsides. In both cases a necessary condition for the formation of the filaments is flux convergence and cancellation at a PIL between separate bipolar regions. As no long-lived filaments form during the periods of the highest rates of flux emergence we infer that surface motions acting on pre-existing coronal fields do play a critical role in the formation of stable filaments through the interaction of multiple bipoles. A key role of these surface motions is to redistribute the helicity, which is seen to emerge in the early stages before the filaments appear (Gaizauskas *et al.*, 1997; Gaizauskas, Mackay, and Harvey, 2001; Mackay and Gaizauskas, 2003; Mackay and van Ballegooijen, 2005), to form the filament channel and axial field of the filament, upon which mass may then be deposited. Convergence and cancellation of flux have also been shown to be important for filament formation, according to the observations reported by Martin (1998) who reviews several clear examples and Gaizauskas (2002) who shows that early on in the solar cycle a unipolar region of flux has to extend 180° around the Sun to interact and cancel with an opposite polarity region before a filament can form.

It is clear from these observations that surface effects play a critical role in forming IFs and QFs (which are long, stable structures). Lites *et al.* (1995) describe a different process for forming short, unstable active-region filaments. By using advanced Stokes polarimetry, magnetic field vectors along part of the PIL within the emerging δ-spot reveal a concave upward or dipped magnetic structure. A small active-region filament forms at this location. The filament is however unstable with a lifetime of only two days.

The observations described here provide evidence for filament formation arising from surface motions that reconfigure already existing coronal fields or, less typically, emerging flux tubes. The important distinction between these cases is the type and location of filaments formed in each case. For the first two cases surface motions play an important role in forming long, stable EBR filaments, the dominant type of filament found at all latitudes on the Sun. In contrast, flux emerging as a δ-spot forms an IBR filament, which is unstable, lasting merely two days.

4.2. Theoretical Models of Filament Formation

Over the years many models have been constructed, each employing a variety of mechanisms to describe the formation of filaments. These models vary from descriptive papers to full numerical MHD simulations and consider two main problems: 1. how to obtain the correct dipped magnetic field configuration with dominant axial magnetic field that follows the hemispheric pattern and 2. the origin of the dense mass. The second question relates more to thermodynamics (Karpen *et al.*, 2001), but this paper, which relates filaments to their underlying magnetic polarities, is relevant to the first group of models. The various models in

Table 3 Models of filament formation.

Surface models		Subsurface models	
Single bipole	Multiple bipoles	Single bipole	Multiple bipoles
van Ballegooijen and Martens (1989)[1,3,4,10]	Kuperus (1996)[1,3,4]	Low (1994)[7]	Priest, van Ballegooijen, and Mackay (1996)[2,3,4,6]
DeVore and Antiochos (2000)[1,4]	Kuijpers (1997)[3,4,8,10]	Rust and Kumar (1994)[7,9]	
	Mackay *et al.* (1998)[3,4,6,8,10]	Gibson (2004)[7,9]	
	Galsgaard and Longbottom (1999)[3,4]	Low and Hundhausen (1995)[7,9]	
	van Ballegooijen, Priest, and Mackay (2000)[1,4,10]		
	Martens and Zwaan (2001)[3,4,10]		
	Lionello *et al.* (2002)[8,10]		
	DeVore, Antiochos, and Aulanier (2005)[1,3,4]		
	Mackay and van Ballegooijen (2005)[1,4,8,10]		
	Welsh, DeVore, and Antiochos (2005)[3,4,8,10]		
	Litvinenko and Wheatland (2005)[3,4,8,10]		
	Yeates, Mackay, and van Ballegooijen (2008)[1,4,8,10]		

that group may be broadly split into two distinct subgroups: those employing surface effects and those employing subsurface effects. Some of these models are listed in Table 3. In this table the surface and subsurface models have also been subdivided into those acting in single or multiple bipolar configurations. This list should only be regarded as a representative, not an exhaustive, set of models. For each of the entries in the table the numbers attached correspond to the various mechanisms that the models employ, as listed in Table 4. From Table 3 it is clear that surface models rely on a variety of mechanisms combined together whereas subsurface models generally rely on the emergence of twisted flux ropes where the filament forms in the dips of the flux rope or U-loop.

Surface mechanisms include differential rotation, shear flows along a PIL (differential rotation being just a weak shear flow), and converging flows onto a PIL. Recent helioseismic observations by Hindman, Haber, and Toomre (2007) show that underneath a well-developed filament strong shear flows may be observed. However, this was after the filament had formed and not during the formation process. For some surface models diffusion of flux towards a PIL with subsequent cancellation plays the role of the converging flow. To produce an axial magnetic field consistent with observations, these flows generally have to occur in a specific order. In contrast to these surface motions, subsurface shear flows have also been employed. In both sets of models magnetic reconnection is generally required to reconfigure the fields; the reconnection may occur either above or below the surface.

Another feature common to both sets of models is flux emergence, but it is used in very different ways. For surface models, magnetic bipoles, emerge either untwisted or twisted,

Table 4 Mechanisms of filament formation.

Surface mechanisms	Subsurface mechanisms
(1) Differential rotation (shear flows)	(2) Subsurface motions
(3) Converging flows	
(4) Magnetic reconnection (atmosphere)	(5) Magnetic reconnection (subsurface)
(6) Flux emergence (bipoles)	(7) Flux emergence (U-loops)
(8) Magnetic helicity	(9) Magnetic helicity
(10) Flux cancellation/diffusion	

are advected across the solar surface and reconfigured with other pre-existing coronal fields. A key element in recent papers describing filament formation is that these bipoles are non-potential and include an initial magnetic helicity (Mackay and van Ballegooijen, 2005; Yeates, Mackay, and van Ballegooijen, 2008). In contrast, flux emergence for subsurface models is presumed to occur in the form of twisted U-loops in which the filament forms as a single entity within an emerging dipped structure.

4.3. Discussion of Present Results in the Context of Previous Observations and Models

From the results in Section 3 it can be clearly seen that the majority of filaments considered in this study (92%) form in magnetic configurations involving multiple bipole interactions, where the filament forms either fully (79%) or partially (13%) above a PIL external to any one bipolar region. Only very few filaments (7%) form in single bipolar configurations along the internal PIL of the bipole. Therefore although none of the models listed in Table 3 can be ruled out it is clear that those involving multiple bipole interactions are the most realistic and appropriate for explaining the large-scale filaments found on the Sun.

From Figure 5 it is clear that IBR filaments show no solar cycle dependence at all. If flux emergence in the form of flux ropes as used by subsurface models was key to their formation then one would expect that IBR filaments should show a strong solar cycle dependence. Simply put, as more bipoles emerge on the Sun there would be a much greater chance of having emerging flux ropes and hence more IBR filaments. As this does not occur, another process must be acting to form filaments (see the following).

If flux rope emergence is an unlikely key to the formation of IBR filaments then it is extremely unlikely that such a process could apply to EBR filaments, which tend to form between distinct bipoles after flux emergence has ended. Again another process must be acting, one closely related to the amount of magnetic flux on the Sun.

The obvious choice is convergence between individual bipoles, resulting in either flux cancellation or coronal reconnection because the rates of convergence increase owing to the increased rate of flux emergence during periods of high activity. During these periods of high activity the most widespread source of convergent flows is the natural expansion of all bipolar pairs as soon as they emerge If these processes are key in explaining the formation of filaments this would lead to an increase in the number of filaments forming between individual magnetic bipoles. In addition, one expects more EBR filaments after cycle maximum than after cycle minimum; after maximum there is still a significant amount of magnetic flux on the Sun so that convergence and cancellation or magnetic reconnection can still take place. This fits the behaviour for EBR filaments that appears in Figure 5.

Therefore convergence and subsequent cancellation or coronal reconnection, not flux rope emergence, are the mechanisms that result in the formation of the majority of large,

stable filaments found on the Sun. The models that apply these techniques in Table 3, those with mechanisms 3, 4, and 10 (Table 4) appear to be the most appropriate. Although this argument is put forward for EBR filaments it also applies to DBR filaments because the flux patterns in which they form are a natural consequence of flux convergence and cancellation but over much longer periods of time. We emphasise that our results arise from an analysis of the large, stable filaments that are found in Solar Geophysical Data. It does not apply to small-scale, unstable filaments found in activity complexes and therefore does not contradict the interpretation of the observations by Lites *et al.* (1995). But it does support the conclusions drawn from the observations by Gaizauskas *et al.* (1997) and Gaizauskas, Mackay, and Harvey (2001).

Because IBR filaments, which are the least common type, show no solar cycle variation those found here probably do not result from flux rope emergence. An alternative explanation for their formation, which in this study generally occurs outside activity complexes, is that they may result from strong surface shearing motions. Evidence for such shearing motions, at least in the later development of a filament, has recently been published by Hindman, Haber, and Toomre (2007). This fits in with the single bipole models discussed in Table 3. Finally, for I/EBR filaments again convergence and cancellation or coronal reconnection may apply but this time strong shear flows may once again be applicable.

5. Summary and Conclusions

We have developed a method to locate where long, stable solar filaments form relative to associated magnetic bipoles. This method employs a wide variety of data: Hα synoptic maps as published in Solar Geophysical Data, Kitt Peak (KP) normal component synoptic magnetograms, KP He 10830 synoptic images, KP full-disk normal component magnetograms, and large-scale Hα images from ORSO. In addition we simulate the surface magnetic field to determine the origin of flux regions at high latitudes from their source regions at lower latitudes over time scales of months.

By these means we are able to extend the earlier work of Tang (1987) to many more filaments sampled over a broad range of latitudes at four different epochs in the solar cycle. We have introduced two additional categories of association between filaments with adjacent magnetic bipoles. The expanded classification scheme distinguishes between differing bipole interactions that could lead to filament formation and signifies which theoretical models are best applicable to those interactions.

The filaments described in Section 2.2 and Figure 2 are classified as internal bipolar region filaments, external bipolar region filaments, internal/external bipolar region filaments, and diffuse bipolar regions filaments, where each classification describes the filament formation location relative to a PIL lying either internally within a single bipole or externally between two bipoles. The number of each type of filament was then considered over four phases of the solar cycle, where two of the phases occurred before and two after cycle maximum.

Our results show that throughout the cycle the most common type of filament is the EBR filament (62%), followed by the DBR filament (17%), then the I/EBR filament (13%), and finally the IBR filament (7%). Thus the majority of filaments on the Sun (92%) occur in magnetic configurations that require multiple bipole interactions. In addition, when the results considered here are reduced into just two classifications, as used by Tang (1987), then agreement is found with the previous results. Therefore by introducing the new classification schemes we shed new light on where filaments form. We find that filaments forming within

a single bipolar configuration are not as common as previously thought; the majority of filaments require multiple bipole interactions.

Furthermore only EBR filaments show any form of solar cycle dependence, with the other three types remaining essentially constant. The number of EBR filaments increases sharply as cycle maximum is approached before decreasing towards cycle minimum. Also more EBR filaments form after cycle maximum than just after cycle minimum.

In contrast, IBR filaments, which form along the internal PIL of a single bipole, show no solar cycle dependence (Figure 5). The absence of variability for this type of filament is inconsistent with the claim that they form via the emergence of magnetic flux ropes as described by Lites *et al.* (1995). We therefore conclude that other effects must play a role in the formation of large-scale IBR filaments.

Because of the strong dependence that we found of EBR filaments on the solar cycle, their formation mechanism must be related to the amount of magnetic flux on the Sun at a given time. With flux emergence playing only an indirect (or minor) role, another mechanism must be acting, but one which can vary across the solar cycle. Convergence resulting in cancellation of flux and the reconfiguration of coronal fields as the result of surface motions are also more likely when their are more bipoles on the Sun. We therefore propose that models that employ these mechanisms are the most plausible for explaining filament formation. Our conclusion does not vitiate the result of Lites *et al.* (1995), who did observe a filament to form during flux emergence. The type of filament analysed by Lites *et al.* (1995), however, was a small, unstable active-region filament whereas the focus in this paper is on large-scale, stable filaments.

On the theoretical side we split models into four types: those employing either single or multiple bipole interactions and those employing either surface or subsurface effects. We found that all four types were consistent with the observations, but those involving multiple bipole interactions were the most effective in explaining the majority of filaments on the Sun.

Present observations suggest that the vast majority of filaments on the Sun form as the result of surface motions. Future work needs to examine filaments over a wide range of latitudes in detail. Filaments that form within activity complexes, ignored in this paper, need to be included as well. Their formation mechanism may well be different.

A better understanding of the formation of filaments requires multiwavelength observations of filaments situated over a wide range of latitudes, from the active-region belts up to the polar crowns. We still do not know for certain whether different formation mechanisms occur at different latitudes on the Sun. To distinguish among the different mass-supply mechanisms, spectral lines from Hα to X rays along with Doppler information are required. Before ordering up this large menu of observations, we must be able to determine where and when both long-lived and short-lived filaments might form. Synoptic data sets should help us predict likely targets. Therefore maintenance of these data sets is vitally important for advancing studies of filament formation.

Acknowledgements The authors would like to thank the referee whose suggestions have greatly improved the paper. The NSO/Kitt Peak data used here are produced cooperatively by NSF/NOAO, NASA/GSFC, and NOAA/SEL. The film archives of high-resolution Hα images from ORSO are maintained at the National Research Council on behalf of the Herzberg Institute of Astrophysics. DHM and ARY would like to thank STFC for financial support.

References

Ambrož, P., Schroll, A.: 2002, *Astron. Astrophys.* **381**, 300.

DeVore, C.R., Antiochos, S.K.: 2000, *Astrophys. J.* **539**, 54.
DeVore, C.R., Antiochos, S.K., Aulanier, G.: 2005, *Astrophys. J.* **629**, 1122.
Galsgaard, K., Longbottom, A.W.: 1999, *Astrophys. J.* **510**, 444.
Gaizauskas, V.: 2002, *Solar Phys.* **211**, 179.
Gaizauskas, V., Zwaan, C.: 1997, *BAAS* **29**, 902.
Gaizauskas, V., Mackay, D.H., Harvey, K.L.: 2001, *Astrophys. J.* **558**, 888.
Gaizauskas, V., Zirker, J.B., Sweetland, C., Kovács, A.: 1997, *Astrophys. J.* **479**, 448.
Gibson, S.: 2004, *Astrophys. J.* **617**, 600.
Hindman, B.W., Haber, D.A., Toomre, J.: 2007, *Astrophys. J.* **653**, 725.
Karpen, J.T., Antiochos, S.K., Hohensee, M., Klimchuk, J.A., MacNeice, P.J.: 2001, *Astrophys. J. Lett.* **553**, L85.
Kuperus, M.: 1996, *Solar Phys.* **169**, 349.
Kuijpers, J.: 1997, *Astrophys. J. Lett.* **489**, 201.
Leroy, J.L.: 1989, In: *Astrophys. Space Sci. Library*, *Dynamics and Structure of Quiescent Solar Prominences* **150**, Kluwer, Dordrecht, 77.
Li, Y., Luhmann, J.: 2006, *Astrophys. J.* **648**, 732.
Lites, B.W., Low, B.C., Martinez Pillet, V., Seagraves, P., Skumanich, A., Frank, Z.A., Shine, R.A., Tsuneta, S.: 1995, *Astrophys. J.* **446**, 877.
Lionello, R., Mikić, Z., Linker, J.A., Amari, T.: 2002, *Astrophys. J.* **581**, 718.
Litvinenko, Y.E., Wheatland, M.S.: 2005, *Astrophys. J.* **630**, 587.
Low, B.C.: 1994, *Phys. Plasmas* **1**, 1684.
Low, B.C., Hundhausen, J.R.: 1995, *Astrophys. J.* **443**, 818.
Mackay, D.H.: 2005, In: Sankarasubramanian, K., Penn, M., Pevtsov, A. (eds.) *Large-scale Structures and their Role in Solar Activity, ASP Conf. Ser.* **346**, 177.
Mackay, D.H., Gaizauskas, V.: 2003, *Solar Phys.* **216**, 121.
Mackay, D.H., van Ballegooijen, A.A.: 2005, *Astrophys. J.* **621**, L77.
Mackay, D.H., Priest, E.R., Gaizauskas, V., van Ballegooijen, A.A.: 1998, *Solar Phys.* **180**, 299.
Martin, S.F.: 1998, *Solar Phys.* **182**, 107.
Martens, P.C., Zwaan, C.: 2001, *Astrophys. J.* **538**, 872.
McIntosh, P.S.: 2002, *Bull. Am. Astron. Soc.* **34**, 737.
Minarovjech, M., Rybansky, M., Rusin, V.: 1998, *Solar Phys.* **177**, 357.
Mouradian, Z., Soru-Escaut, I.: 1994, *Astron. Astrophys.* **290**, 279.
Priest, E.R., van Ballegooijen, A.A., Mackay, D.H.: 1996, *Astrophys. J.* **460**, 530.
Rust, D.M., Kumar, A.: 1994, *Solar Phys.* **155**, 69.
Tandberg-Hanssen, E.: 1995, In: *The Nature of Solar Prominences* **358**, Kluwer, Dordrecht.
Tang, F.: 1987, *Solar Phys.* **319**, 163.
van Ballegooijen, A.A., Martens, P.C.H.: 1989, *Astrophys. J.* **343**, 971.
van Ballegooijen, A.A., Priest, E.R., Mackay, D.H.: 2000, *Astrophys. J.* **539**, 983.
Welsch, B.T., DeVore, C.R., Antiochos, S.K.: 2005, *Astrophys. J.* **634**, 1395.
Yeates, A.R., Mackay, D.H., van Ballegooijen, A.A.: 2007, *Solar Phys.* **245**, 87.
Yeates, A.R., Mackay, D.H., van Ballegooijen, A.A.: 2008, *Solar Phys.* **247**, 103. doi:10.1007/s11207-007-9097-0.